

## INVESTIGATION OF CONTINUOUS FIBER-REINFORCED TRIPLY PERIODIC MINIMAL SURFACES (TPMS) FOR HIGH-PERFORMANCE ENERGY ABSORPTION APPLICATIONS

Bence Szederkényi<sup>1\*</sup>, Norbert K. Kovács<sup>1,2</sup>, Tibor Czigány<sup>1,3</sup>

<sup>1</sup>Department of Polymer Engineering, Faculty of Mechanical Engineering, Budapest University of Technology and Economics, Muegyetem rkp. 3., H-1111 Budapest, Hungary

<sup>2</sup>MTA-BME Lendület Lightweight Polymer Composites Research Group, Muegyetem rkp. 3., H-1111 Budapest, Hungary

<sup>3</sup>HUN-REN-BME Research Group for Composite Science and Technology, Muegyetem rkp. 3., H-1111 Budapest, Hungary

\*corresponding author: bszederkenyi@edu.bme.hu

### Abstract

Homogeneous and quasi-homogeneous cell structures, including triple-periodic minimal surfaces (TPMS), are crucial in engineering, particularly in lightweight energy absorption applications. While typically made from metals or polymers, the exploration of polymer composites in cellular systems is increasing, driven by additive manufacturing technologies. High-performance energy-absorbing systems often use continuous carbon fiber-reinforced composites embedded in a thermoset matrix. Despite their potential, current literature focuses on short-fiber composites in TPMS systems, with limited studies on continuous fiber placement. We used a Markforged Mark Two 3D printer to explore various cell structures and reinforcement patterns for continuous fibers. The paper investigates the energy absorption capabilities of these structures to enhance their specific energy-absorbing capability, contributing to the development of modern energy-absorbing structures.

**Keywords:** 3D printed CFRP, Cellular structures, TPMS, Energy absorption, SEA

### 1. Introduction

The purpose of energy-absorbing structures is to mitigate the momentary, impulse-like effects of dynamic impact by dissipating energy. This process leads to structural deformation, increasing the duration of the load while potentially reducing its intensity significantly by orders of magnitude as energy is absorbed through various structural transformations. The main design parameters for energy-absorbing devices are maximum force and maximum deceleration which the protected objects are capable of withstanding [1]. Currently, energy absorption applications primarily utilize polymer and metal foams and honeycomb structures, exploiting their adjustable porosity and typically plastic properties within these applications. Additionally, with the emergence of additive manufacturing (AM) technologies, tailorable properties of regular cell structures have become a significant research area in energy absorption applications. Cellular structures respond to compressive loads with a consistent plateau phase, offering a predictable maximum force until critical densification. However, a similar characteristic can also be achieved with materials incapable of plastic deformation, such as fiber-reinforced composites [2–5].

#### 1.1. Composites and energy absorption

The application of composites for energy absorption purposes has been a researched area since the 1970s, with its findings applied in numerous critical areas, including helicopter and race car crash zones [6–9]. These structures typically consist of thin-walled, closed-profile systems, primarily tube-like, oriented with their long axis toward the expected impact [10–12]. During crushing, a progressive mechanism can be initiated to stabilize the otherwise catastrophic and unstable response of fiber-reinforced composite specimens. This mechanism advances synchronously with the propagation of the crush zone, a process referred to as fragmentation. The research by Starbuck *et al.* [13] indicates that in the energy-absorption applications of composites, fiber failure is the dominant energy-absorbing mechanism, followed by various crack propagation and fiber bending mechanisms.

## 1.2. Applications of triply periodic minimal surfaces (TPMS) in energy absorption

In recent years, the utilization of TPMS structures for energy absorption has emerged as a prominent convergence of AM technologies and high-performance, lightweight structures. In these domains, where spatially adjustable properties are increasingly important, TPMS structures have gained significant attention. [14–17]. We selected these cellular systems for our study due to their self-supporting structures, facilitating support-free printing in subsequent processes. Moreover, the mechanical properties of various TPMS structures are extensively documented in the literature [18, 19].

Our objective was to develop hybrid, fiber-reinforced cellular structures that efficiently absorb energy through fragmentation processes, achieved by strategically placed fiber reinforcements. We conducted quasi-dynamic compression tests on various TPMS cell structures using combinations of Markforged's PA6 and Onyx materials alongside continuous carbon fiber to accomplish this. We evaluated the impact of different fiber placement strategies on the energy absorption properties of reinforced structures. We also explored the influence of infill strategies provided by slicing software on unreinforced structures.

## 2. Methodology

### 2.1. Selection of test geometry and fiber reinforcement design

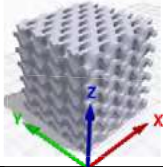


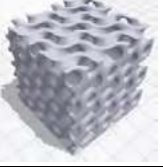
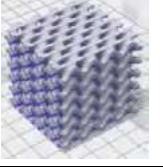
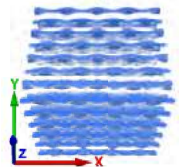
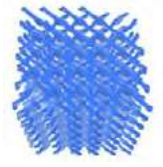
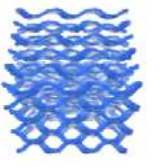
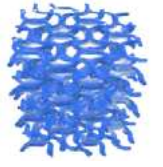

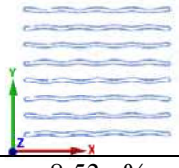
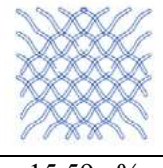
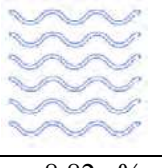
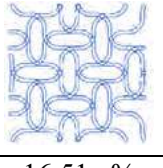
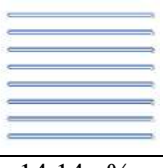
During the TPMS cell structure selection process, we established three key criteria. Firstly, the geometry must be manufacturable without support material, using the chosen material extrusion (MEX) technology. Secondly, the structure should feature longer, uninterrupted cross-sections perpendicular to the main building direction, facilitating continuous fiber placement along its entire length (Table 1). Lastly, we aimed to maximize the geometric energy absorption performance of TPMS cells by selecting structures with optimal specific properties. Building on the research by Kladovasilakis *et al.* [18] and Saleh *et al.* [19], we further analyzed the gyroid (G) and diamond (D) structures to meet these objectives. The compression test specimens were selected as cubes by relevant standards [20]. To mitigate edge effects, we placed 3x3x3 unit cells within these specimens, following literature recommendations [21]. The choice of cube edge length was primarily dictated by the narrowest fiber-reinforced cross-section, determined to be 2.8 mm based on literature data [22] and our own investigations. Consequently, the compression-tested cube had an edge length of 45 mm, with unit cell edges measuring 15 mm, resulting in a relative density of approximately 37%.

Achieving suitable energy absorption characteristics relies on stable, progressive failure processes in the fiber-reinforced region, where continuous fibers break into smaller fragments. In our experiments, we positioned fibers parallel to the loading direction or at angles of  $\pm 45$  degrees. Fiber placement was restricted to printed layers, ensuring the creation of consistent, identifiable reinforcement with uniform fiber orientation. Thus, for specimens with 0-degree reinforcement, every 60 layers included ten continuous fiber-filled layers spanning the entire cross-section. In specimens reinforced at  $\pm 45$  degrees, this frequency doubled, with ten continuous fiber-filled layers appearing in every 30 layers, resulting in approximately 8 v% and 16 v% fiber content within the material-filled volume.

To achieve the desired fiber reinforcement orientation, we rotated the elemental cells of the cell structure, resulting in corresponding rotations of characteristic cross-sections where the reinforcement is placed. Consequently, four different reinforced structures were created (Table 1), labelled as D0, D45, G0, and G45, denoting the cellular structure of Gyroid (G) or Diamond (D) and the dominant fiber direction within each cell type (0 or  $\pm 45$ ). Here, the loading direction aligns with the 0-degree fiber direction, coinciding with the X-axis in our notation system.

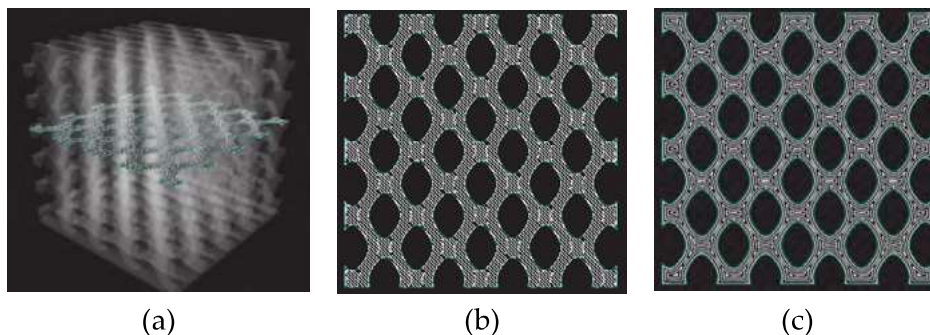
We hypothesized that the progressive failure mechanism heavily depends on the local curvature of reinforcement paths. Slight waviness induces bending-dominated failure in the structure rather than initiating fragmentation-dominated failure modes, leading to more effective energy absorption characteristics. As shown in Table 1 (G0-D45), reinforcements representing dominant fiber directions exhibit varying degrees of waviness in all cases.

**Table 1.** Various TPMS structures and fiber reinforcement were examined. The X-axis represents the loading direction, while the Z-axis denotes the printing build direction.

	D0	D45	G0	G45	D0 masked	
Weight	PA	52.7 g	51.8 g	43.9 g	44.5 g	-
	Onyx	51.5 g	52.5 g	44.2 g	44.6 g	-
	CCF	52.2 g	51.1 g	43.5 g	43.7 g	52.8 g
Cell structure						
Reinforcement paths within the specimen						
Reinforcement repeating unit/layer inside the specimen						
Fiber content	8.53 v%	15.59 v%	8.82 v%	16.51 v%	14.14 v%	

To mitigate this effect and enhance energy absorption, we introduced an additional diamond-based structure (D0\_masked), where fiber reinforcement was implemented as a separate geometry within the specimen, forming perfectly straight columns. This was achieved by post-merging the unreinforced and reinforced geometries, created separately in the slicing software and consolidated into G-code.

Alongside specimens with continuous fiber reinforcement, we manufactured a series of pure PA and a series of Onyx (short CF-filled PA) specimens to isolate the effect of fiber reinforcement. Markforged's slicing software, Eiger, a closed industrial system, allows for bare fiber reinforcement placement only if the "exposed infill" beta option is enabled. This feature skips the placement of wall layers and prints only the internal structure of the test specimen, possible with raster infill when using 100% infill (Figure 1 (b)). Consequently, the series without fiber reinforcement was also created with the use of raster infill, with the "exposed infill" option enabled. To further investigate the infill strategy, we made additional test specimens from Onyx with a concentric infill strategy (Figure 1 (c)). The effect of the infill strategy was exclusively examined for the D0 specimens. For the printing parameters, refer to Table 2.



**Figure 1.** Infill strategies: A general cross-section (a), which can be filled with a raster (b) or concentric (c) infill pattern.

**Table 2.** Manufacturing parameters of the compression test specimens

	G0, G45, D0, D0 masked, D45	D0 concentric
Layer thickness	0,125 mm	0,125 mm
Nozzle diameter	0,4 mm	0,4 mm
Infill ratio	100%	100%
Number of walls	0	0
Number of bottom/ top layers	0	0
Reinforcement path-planning strategy	concentric, one loop/-	-
Material deposition strategy in XY plane	raster in $\pm 45^\circ$	concentric

### 2.2. Test environment and parameters

The quasi-dynamic compression tests were conducted on a Zwick Z250 universal testing machine at a maximum achievable loading rate of 600 mm/min. The tests were performed up to 85% engineering strain or a maximum load of 200 kN. The specimens were not conditioned, and air temperature during testing was 21°C with a relative humidity of 48%.

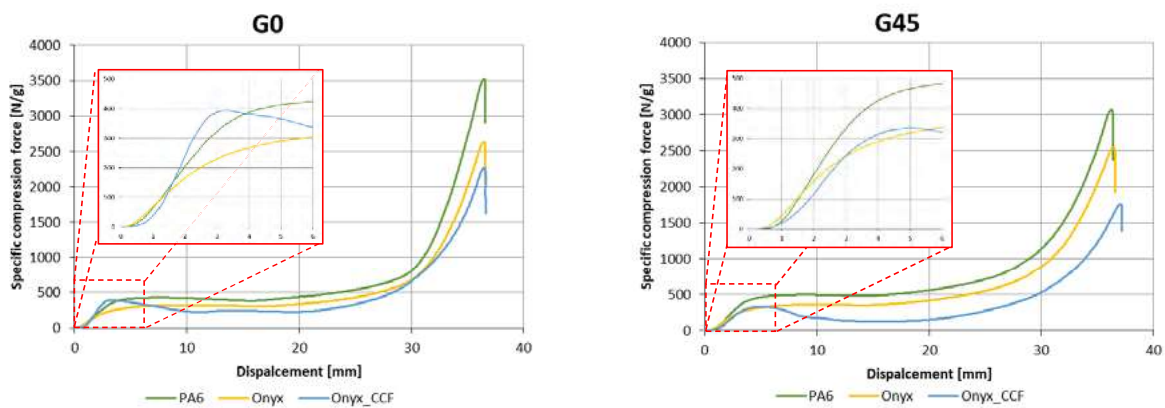
For comparability of the test results, all data is presented normalized to the mass of the respective specimen. Detailed descriptions of the examined parameters can be found in Table 3.

Table 3. Parameters examined during the tests

Designation	Abbreviation	Unit	Determination methodology
Specific energy absorption capability	SEA	J/g	Integration of the force–displacement curve up to the most efficient energy absorption point, followed by normalization with the mass of the specimen (For further information refer to [23])
Specific compression force	F*	N/g	Normalized compressive force with respect to the mass of the specimen.
Specific plateau force	F* <sub>plat</sub>	N/g	Average plateau force normalized by the mass of the specimen.
Specific stiffness	E*	MPa/g	The slope of the straight line fitted to the first linear segment of the engineering stress–engineering strain curve, normalized by the mass of the specimen.

### 3. Results

For better clarity in the presentation of the test results, we depicted the various cell structures on separate diagrams. Additionally, we detailed the initial loading phase in the diagrams. Figure 2 illustrates these compression diagrams.



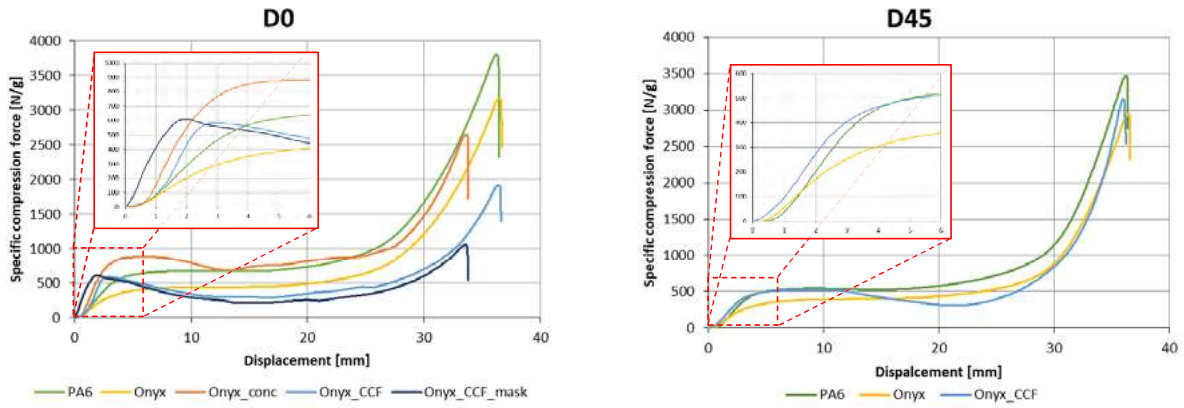


Figure 2. Specific compression force-displacement curves of the test specimens.

From the curves shown in Figure 2, the parameters listed in Table 3 were then calculated for all test specimens. These were then summarized and displayed in the bar chart in Figure 3. To allow for a common diagram, all metrics were expressed as percentages relative to the G0 specimen made of PA6. However, the absolute values were also indicated on the chart in addition to the relative values.

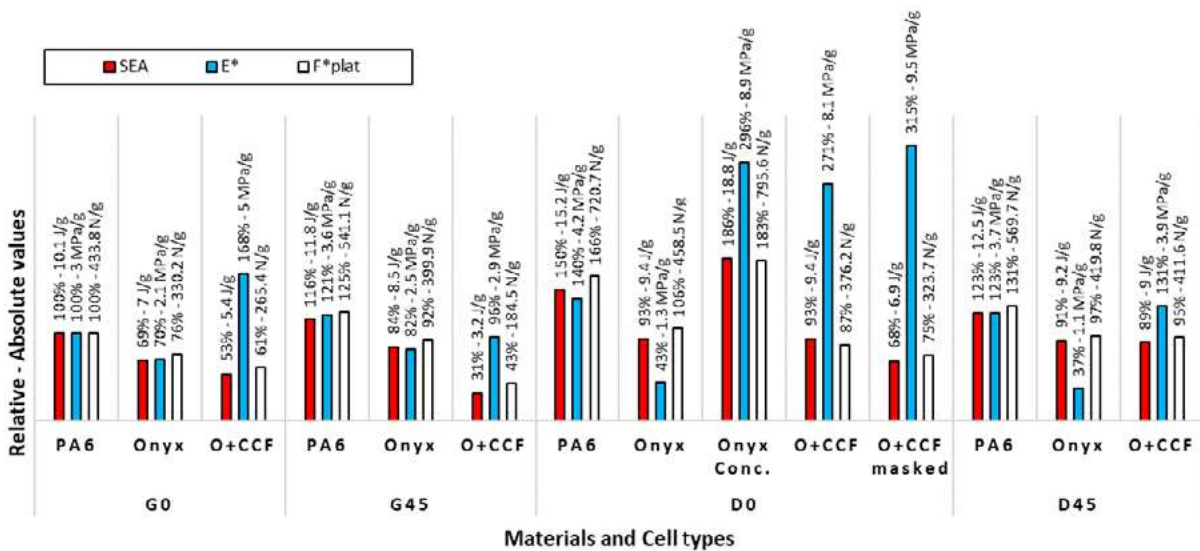
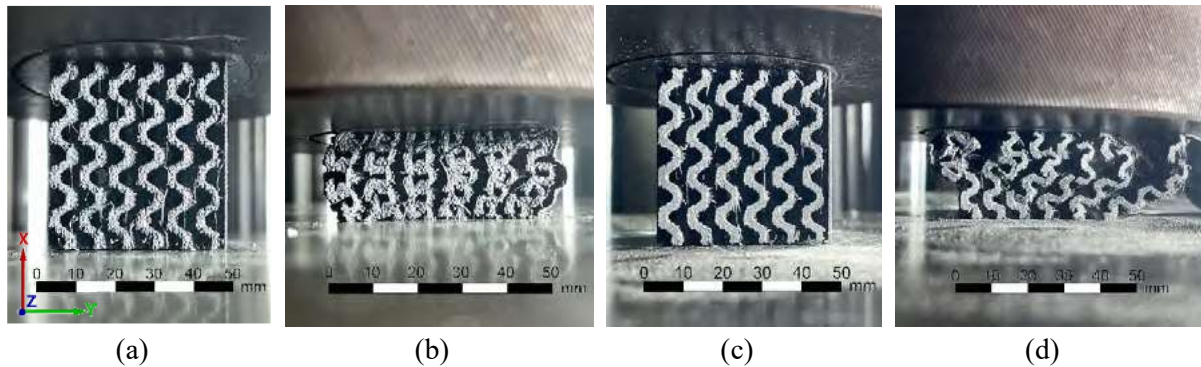


Figure 3. The column chart shows all the results of the tested structures, presenting the relative and absolute performance of each specimen, values normalized to the G0 PA6 structure.

The specimens exhibited consistent failure characteristics across all cell types and orientations, where the PA6 and Onyx specimens remained intact throughout the loading phase, while the fiber-reinforced specimens separated along their length within the reinforced cross-section. Figure 4 illustrates failure typical of matrix-only materials (a, b) compared to the fiber-reinforced structures (c, d).



**Figure 4.** Failure characteristic of the axially loaded Schwarz-Diamond cellular structure in the case of short fiber–reinforced PA6 (Onyx) matrix material, where (a) is the undeformed state and (b) shows the  $\sim 60\%$  compressive strain state. The axially loaded Schwarz-Diamond cellular structure with continuous fiber reinforcement showed weak interlayer adhesion, where (c) is the undeformed state and (d) shows the  $\sim 60\%$  compressive strain state.

#### 4. Discussion and conclusions

Based on the measurement results, the following conclusions were drawn:

1. Clear rankings were established among the examined structural types in cases without continuous fiber reinforcement, extending across all measured parameters. The ranking is as follows: The best was D0, followed by D45, G45 and G0.
2. Fiber–reinforced specimens exhibited a significant average increase of 81% in specific modulus compared to versions made from PA6 for fiber reinforcements corresponding to the  $0^\circ$  loading direction (G0; D0). The structurally regular  $0^\circ$  (D0 masked) fiber–reinforced specimen exhibited an even higher 126% increase in specific modulus.
3. Short-fiber–reinforced Onyx specimens underperformed the pure PA6 structures in terms of all metrics, with average specific modulus reductions of 32% for gyroid (G0, G45) structures and 70% for diamond (D0, D45) structures. In the case of specific plateau forces, this difference averaged 28% across all specimen types while averaging 31% for specific energy absorption. This discrepancy likely stems from the similar ratios between the moduli of pure materials and the lower failure deformation threshold of Onyx, attributed to its high content of inner friction reducers and other additives affecting stiffness.
4. The difference between raster and concentric printing yielded unexpected deviations favoring concentric printing. Among structures made from Onyx material, there was a 585% difference in specific modulus, a 77% difference in specific plateau force, and a 100% difference in SEA values. This significant difference underscores the importance of choosing continuous infill in energy absorption applications, where rasterized infill intermittently builds the cross-section and has a pronounced detrimental effect.
5. The SEA value of the regular  $0^\circ$  (D0 masked) specimen was 37% lower than that of the slightly wavy fiber–reinforced (D0) specimen, likely due to the design created by the combination of two separate pieces on the printing bed during manufacturing, presumably degrading layer adhesion. Additionally, the phenomenon can be explained by the greater lateral force component after stability loss, which caused the structure to separate sooner.
6. Regarding SEA values, the fiber–reinforced specimens consistently underperformed compared to the Onyx and PA6 specimens, with an average value of 47% compared to PA6. This can be explained with the phenomenon presented in Figure 4, where it is clear that while the pure matrix material specimens remained intact throughout the entire loading range, the fiber–reinforced specimens could not resist the simultaneously emerging axial and lateral force components and delaminated and separated due to weak interlayer adhesion. Consequently, they contributed much less to the energy absorption process when deviating from the loading direction. Thus, the desired fiber fragmentation processes fail to initiate properly in the examined specimens,

indicating that continuous fiber reinforcement has not been adequately utilized for energy absorption in the presented cases.

## 5. Limitations and future improvements

In our study, only one specimen type was manufactured for each test. Thus, our observations and conclusions lack statistical certainty. Supplementary tests would be necessary to establish statistical significance, a task we plan to undertake in the future. Concerning the masked specimen, we relied solely on assumptions regarding interlayer adhesion values, which warrant further investigation under standardized conditions. Moreover, based on the observations outlined in sections 4–6 of Conclusion, it is evident that the most critical parameter requiring development is the integrity of the cellular structure. It ensures adequate support for the fiber reinforcement, even at substantial load states. This may entail enhancing the interfacial adhesion of the fiber reinforcement or implementing macro-level methods, such as radially placed fiber reinforcement. Investigating and improving these parameters could be the foundation for future research.

## Acknowledgments

The research reported in this paper was supported by the National Research, Development, and Innovation Office (NRDI, Hungary) through grants OTKA FK134336 and OTKA K 138472.

Project no. TKP-6-6/PALY-2021 has been implemented with the support provided by the Ministry of Culture and Innovation of Hungary from the National Research, Development and Innovation Fund, financed under the TKP2021-NVA funding scheme.

The project 2022-2.1.1-NL-2022-00012 has been implemented with the support provided by the Ministry of Culture and Innovation of Hungary from the National Research, Development and Innovation Fund, financed under the 2022-2.1.1-NL Creation of National Laboratories, Complex Development funding scheme.

Bence Szederkényi expresses appreciation for the support of the Doctoral Excellence Fellowship Programme (DCEP), which is funded by the National Research Development and Innovation Fund of the Ministry of Culture and Innovation and the Budapest University of Technology and Economics under a grant agreement with the National Research, Development and Innovation Office.

Norbert Krisztián Kovács expresses appreciation for the support of the ÚNKP-23-5-BME-466 New National Excellence Program of the Ministry for Culture and Innovation from the source of the National Research, Development and Innovation Fund and the János Bolyai Research Scholarship of the Hungarian Academy of Sciences.

## References

- [1] Mamalis A. G., Robinson M., Manolacos D. E., Demosthenous G. A., Ioannidis M. B., Carruthers J. Review Crashworthy capability of composite material structures. *Composite Structures*, 37:109–134, 1997.
- [2] Özen İ., Gedikli H., Aslan M. Experimental and numerical investigation on energy absorbing characteristics of empty and cellular filled composite crash boxes. *Engineering Structures*, 289:116315, 2023.
- [3] Mamalis A. G., Manolacos D. E., Demosthenous G. A., Ioannidis M. B. The static and dynamic axial crumbling of thin-walled fibreglass composite square tubes. *Composites Part B: Engineering*, 28:439–451, 1997.
- [4] Rzyńska G., Gieleta R. Effect of Test Velocity on the Specific Energy Absorption under Progressive Crushing of Composite Tubes. *Advances in Science and Technology Research Journal*, 14:94–102, 2020.
- [5] Mamalis A. G., Manolacos D. E., Demosthenous G. A., Ioannidis M. B. Analysis of failure mechanisms observed in axial collapse of thin-walled circular fibreglass composite tubes. *Thin-Walled Structures*, 24:335–352, 1996.
- [6] Heimbs S., Strobl F. Crash Simulation of an F1 Racing Car Front Impact Structure. *Proceedings of 7th European LS-DYNA Conference*, 1–8, 2009.

- [7] Boria S., Obradovic J., Belingardi G. Experimental and numerical investigations of the impact behaviour of composite frontal crash structures. *Composites Part B: Engineering*, 79:20–27, 2015.
- [8] Bisagni C., Di Pietro G., Fraschini L., Terletti D. Progressive crushing of fiber-reinforced composite structural components of a Formula One racing car. *Composite Structures*, 68:491–503, 2005.
- [9] Kohlgrueber D., Kamoulakos A. Validation of Numerical Simulation of Composite Helicopter Sub-floor Structures under Crash Loading. *Dieter Kohlgrüber German Aerospace Center (DLR) Institute of Structures and Design D-70569 Stuttgart, Germany Argiris Kamoulakos Engineering Systems Int.*, 1998.
- [10] Matzenmiller A., Schweizerhof K. Crashworthiness simulations of composite structures - a first step with explicit time integration. In *Nonlinear Computational Mechanics: State of the Art*, Springer, Berlin, 1991.
- [11] McGregor C., Zobeiry N., Vaziri R., Poursartip A., Xiao X. Calibration and validation of a continuum damage mechanics model in aid of axial crush simulation of braided composite tubes. *Composites Part A: Applied Science and Manufacturing*, 95:208–219, 2017.
- [12] Hull D. A unified approach to progressive crushing of fibre-reinforced composite tubes. *Composites Science and Technology*, 40:377–421, 1991.
- [13] Starbuck J. M., Adams D. O., Courteau M. Energy absorbing damage mechanisms in progressive crushing of composite tubes. In *Proceedings of the 32nd Technical Conference of the American Society for Composites*, 2:1419–1432, 2017.
- [14] Yang L., Li Y., Wu S., Chen P., Wu H., Su J., Wang H., Liu J., Yan C., Shi Y. Tailorable and predictable mechanical responses of additive manufactured TPMS lattices with graded structures. *Materials Science and Engineering: A*, 843:143109, 2022.
- [15] Alkebsi E. A. A., Ameddah H., Outtas T., Almutawakel A. Design of graded lattice structures in turbine blades using topology optimization. *International Journal of Computer Integrated Manufacturing*, 34:370–384, 2021.
- [16] Sánchez J. M., Weems E., Hu H. Coupled Field-Driven Design and Numerical Simulation for Engineering Education. *Proceedings of 2023 ASEE Midwest Section Conference*, 2023.
- [17] Xu Z., Razavi S. M. J., Ayatollahi M. R. Functionally Graded Lattice Structures: Fabrication Methods, Mechanical Properties, In *Failure Mechanisms and Applications*, Elsevier, New York, 2022.
- [18] Kladovasilakis N., Tsongas K., Kostavelis I., Tzovaras D., Tzetzis D. Effective mechanical properties of additive manufactured triply periodic minimal surfaces: experimental and finite element study. *International Journal of Advanced Manufacturing Technology*, 121:7169–7189, 2022.
- [19] Saleh M., Anwar S., Al-Ahmari A. M., Alfaify A. Compression Performance and Failure Analysis of 3D-Printed Carbon Fiber/PLA Composite TPMS Lattice Structures. *Polymers*, 14:4595, 2022.
- [20] ISO 844: Rigid cellular plastics. Determination of compression properties, 2021.
- [21] Peng C. Novel Lattice Structures Based on Triply Periodic Minimal Surfaces. *RMIT University, College of Science, Technology, Engineering and Maths, School of Engineering College*, Phd Thesis, 2022.
- [22] Catapano A., Montemurro M., Balcou J.-A., Panettieri E. Rapid Prototyping of Variable Angle-Tow Composites. *Aerotecnica Missili & Spazio*, 98:257–271, 2019.
- [23] Lu G., Yu T. *Energy Absorption of Structures and Materials*. CRC Press, Boca Raton, 2003.